Article

The Role of Non-Framework Lewis Acidic Al Species of Alkali-Treated HZSM-5 in Methanol Aromatization

Po-Chen Lai [1], Chi-Ying Hsieh [1], Chao-Huang Chen [2] and Yu-Chuan Lin [1,*] (iD)

[1] Department of Chemical Engineering, National Cheng Kung University, Tainan 70101, Taiwan;
   brucelai999@gmail.com (P.-C.L.); o12345445@yahoo.com.tw (C.-Y.H.)
[2] Division of Chemical Engineering, Material and Chemical Research Laboratories,
   Industrial Technology Research Institute, Hsinchu 30011, Taiwan; chchen1031@itri.org.tw
[*] Correspondence: yclin768@mail.ncku.edu.tw; Tel.: +886-6-275-7575 (ext. 62668)

Abstract: Mesoporous HZSM-5 prepared by alkaline treatment (also termed desilication) has drawn significant attention due to its potential in large-scale production and in versatile applications, such as separation and catalysis. Alkali-treated HZSM-5 contains considerable amounts of non-framework (amorphous) Lewis acidic Al species on the external surface, and is deemed to be essential in affecting its catalytic performances. This study intends to clarify the catalytic nature of amorphous Al species of alkali-treated HZSM-5 in methanol aromatization. Physicochemical characterizations, including N_2 adsorption, scanning electron microscopy (SEM), X-ray diffraction (XRD), magic-angle-spinning nuclear magnetic resonance (MAS NMR), inductively coupled plasma (ICP) analysis, NH_3 temperature-programmed desorption (TPD), and methanol-TPD, were performed. The outcomes showed that non-framework Al promotes the hydride transfer in mesoporous HZSM-5, thereby facilitating the aromatization reaction. Among aromatic products, durene can be promoted by non-framework Al through methylation/transalkylation of other aromatics, particularly xylenes, instead of being promoted by reduced space confinement in mesoporous HZSM-5.

Keywords: aluminum; alkaline treatment; Lewis acid; HZSM-5; methanol

1. Introduction

Designing and utilizing hierarchically-structured (or mesoporous) HZSM-5 zeolites is burgeoning. According to the Web of Science database using "hierarchical", "HZSM-5", and "zeolites" as keywords, the number of relevant papers published per year increased approximately threefold from 2012 (40 papers) to 2016 (121 papers). This increase can be attributed to the great potential of hybrid meso-/microporous HZSM-5 in industrial applications, such as separation/adsorption, ion exchange, and heterogeneous catalysis [1]. The success of the applications of multilevel porous HZSM-5 is mainly caused by the auxiliary mesoporosity, which can enhance the accessibility of the inner space in micropores [2]. Viewpoints on, and assessments of, fabrication, characterization, and the engineering of mesoporous HZSM-5 have already been documented in excellent reviews [3–9].

Hierarchical ZSM-5 can be synthesized through a bottom-up (constructive) or a top-down (destructive) method: the former is to impede the crystal growth or to introduce a mesoporous template in the preparation; the latter is to extract/rearrange atoms of Si and Al (demetallation) from the framework [10,11]. By comparison, the destructive method using alkaline treatment (desilication) is more applicable, reliable, and cost-effective (e.g., this method does not use any expensive template as the bottom-up method does [10]) in large-scale production. Pilot-scale production (35 kg per batch in a 1.5 m^3 reactor) of desilicated HZSM-5 catalysts in practicable granular forms has been successfully demonstrated by Pérez-Ramírez and his coworkers [8,12].

Alkali-treated HZSM-5 possesses enhanced strength, density, distribution of acid sites, and improved reactant/product diffusivities in its mesoporous network compared to pristine HZSM-5. Two types of Al sites, i.e., tetrahedrally-coordinated AlO_4^- and octahedral Al species, are coexistent in alkali-treated HZSM-5. Tetrahedral AlO_4^- sites are located mostly in the framework of microporous cavities in HZSM-5. Lately, the location of framework Al has been reported to affect the distribution of products significantly in methanol conversion: AlO_4^- located in channel intersections promotes the formation of aromatics; AlO_4^- located in the sinusoidal and straight channels advances the formation of alkenes [13]. Octahedral Lewis acidic Al can be deposited on the external surface of HZSM-5 in a basic medium [14,15]. Many groups have observed the advantages of non-framework (amorphous) Al species of desilicated HZSM-5 in conversions of methanol [14], butane [16], and hexane [17], and have reported the higher aromatics yield and the longer catalyst lifespan of alkaline-treated HZSM-5 than those of the parent HZSM-5. Nevertheless, there is still limited information about the physicochemical nature of amorphous Al species deposited on the external surface of alkali-treated HZSM-5, especially the species' catalytic properties [14,16].

This study aims to explore the influences of non-framework Lewis acidic Al species of alkali-treated HZSM-5 in methanol to aromatics (MTA). A head-to-head comparison of commercial HZSM-5 (Si/Al = 40), alkali-treated HZSM-5, and HZSM-5 treated first by alkali, and then by acid, were conducted, and their behavior was evaluated in MTA. The results showed that aromatics yield can be improved by the reduced transport resistance of the mesoporous structure, and by non-framework Lewis acidic Al species as well.

2. Results and Discussion

Table 1 lists the porosities of the tested catalysts. The total surface area, the micropore surface area, and the micropore volume declined in the order HZ > HZ-D > HZ-DA, while the total pore volume, the mesopore surface area, and the mesopore volume had an inverse trend. Using HZ as the reference, the fractional change of porosity was calculated (see Figure S1 in Supplementary Materials). Mesopores and total volumes increased substantially (more than 100%) for HZ-D and HZ-DA, compensating with minor losses of the total surface area (<5%), the micropore surface area (<17%) and the micropore volume (<17%). Such a trade-off allows the diffusivities of reactants and products to be improved greatly, and is known to have positive effect in aromatics yield in MTA [18–20].

Table 1. Porosities of tested catalysts.

Catalyst	S_{BET} (m^2/g)	S_{micro} [1] (m^2/g)	S_{meso} [2] (m^2/g)	V_{total} [3] (cm^3/g)	V_{micro} [1] (cm^3/g)	V_{meso} [4] (cm^3/g)
HZ	519.4	296.3	223.2	0.299	0.123	0.176
HZ-D	502.2	252.2	250.0	0.610	0.105	0.505
HZ-DA	493.4	241.5	251.9	0.769	0.103	0.666

[1] Estimated through the *t-plot* method. [2] Calculated from S_{BET}-S_{micro}. [3] Volume adsorbed at p/p_0 = 0.9. [4] Calculated from V_{total}-V_{micro}.

Figure 1 displays N_2 isotherms and Barrett-Joyner-Halenda (BJH) mesopore size distributions. Compared to HZ, all samples displayed Type VI isotherms with a more pronounced hysteresis loop, particularly HZ-D and HZ-DA. The mesopore PSD plots showed a main peak at approximately 4 nm for HZ, while HZ-D and HZ-DA seemed to be a bimodal distribution, showing two responses at 4 nm and 10–20 nm regions. The response at 4 nm is an artifact of a closure point of a hysteresis loop; it is not a reflection of actual 4 nm pores [21]. The intrinsic mesoporosity of HZ listed in Table 1 should be attributed to slit-shaped intercrystalline void less than 4 nm wide. Hence, the employed alkaline treatment is effective in cultivating intercrystalline mesopores in a 10–20 nm range [11]. A close inspection showed that HZ-D had the mesopore size at 11.5 nm; HZ-DA, 18.7 nm. The difference in the mesopore size of HZ-D and HZ-DA is related to the removal of amorphous Al debris by acid wash [22],

that can reopen partially occluded mesopores. Indeed, compared to HZ-D and parent HZSM-5 (HZ), higher mesoporosity of HZ-DA should have lower mass transport resistance.
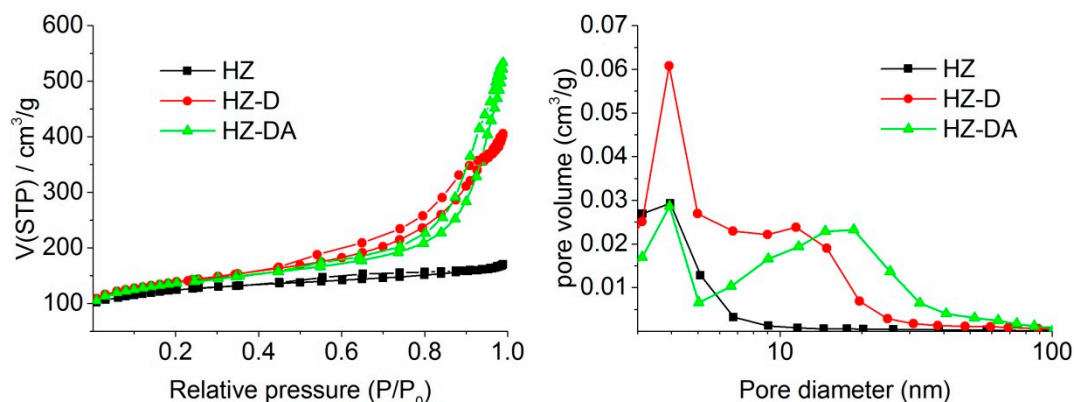

Figure 1. N_2 isotherms and the distribution of pore sizes of tested catalysts.

Figure 2 exhibits the SEM images of HZ, HZ-D, and HZ-DA. Coffin-shaped ZSM-5 crystals with sharp kinks and edges could be observed on HZ. As for HZ-D and HZ-DA, crystals with rounded edges and corners were identified, accompanying some cracks and pinholes on the surface. This implies the newly-developed mesoporous architecture could be synthesized and the intrinsic mesopores of intercrystalline void space could be destroyed through the alkaline treatment.
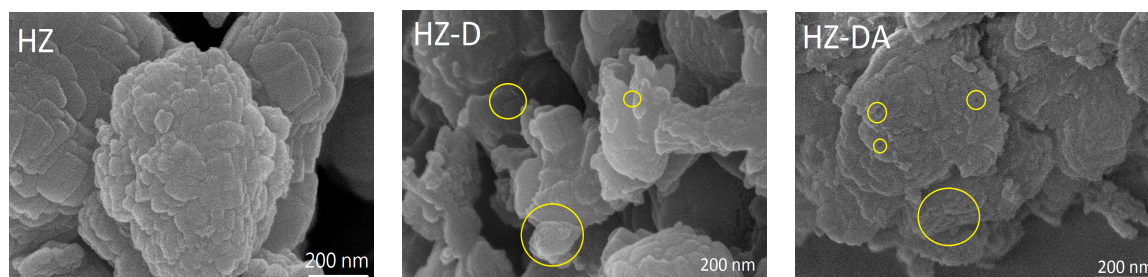

Figure 2. SEM micrographs of HZ, HZ-D, and HZ-DA.

Figure 3 shows the XRD patterns of tested ZSM-5 catalysts. All catalysts displayed the Mordenite Framework Inverted (MFI) structure with different crystallinities estimated according to the relative response of plane (501) at 23.3° using HZ as the reference [23]. Compared to HZ, HZ-D and HZ-DA showed lower crystallinities (approximately 80%), implying parts of the zeolite skeleton could be damaged in the basic medium.

Figure 4 exhibits the ^{27}Al NMR spectra. The resonances of framework tetrahedral Al (Al(Td), 54 ppm) and non-framework octahedral Al (Al(Oh), 0 ppm) can be specified [24]. The relative composition of these two Al species was calculated based on the area under the response. HZ had 90% framework Al(Td) with 10% non-framework Al(Oh). A more than two-fold increase of Al(Oh) (from 10% to 23%) and a substantial decrease of Al(Td) (from 90% to 77%) were observed on HZ-D. This variation indicates the presence of alkaline-induced Lewis acidic Al species on the outer surface [22]. As for HZ-DA, Al(Td) seemed to grow back from 77% to 87% with Al(Oh) that decreased from 23% to 13%. The increased Al(Td) ratio was possible caused by a re-alumination process through which some extra-framework Al could be reinserted into the ZSM-5 framework in an acidic environment [25,26], while the decrease of Al(Oh) indicates that some extra-framework Al species were removed from the outer surface. Briefly, HZ-D had the highest compositions of Al(Oh) and the lowest compositions of Al(Td) among tested catalysts.
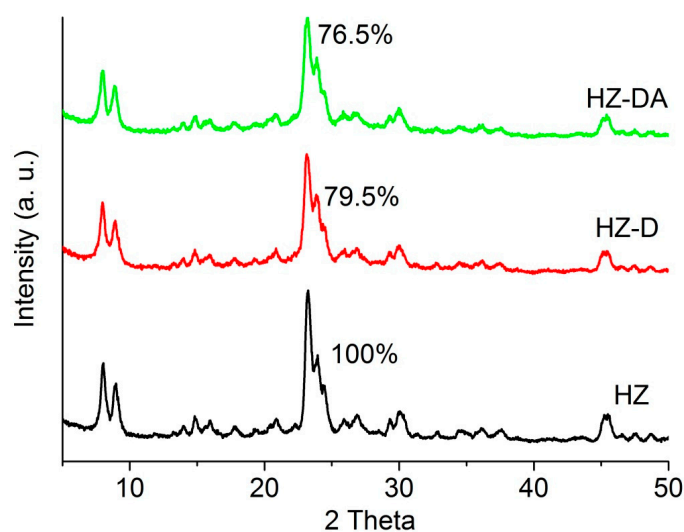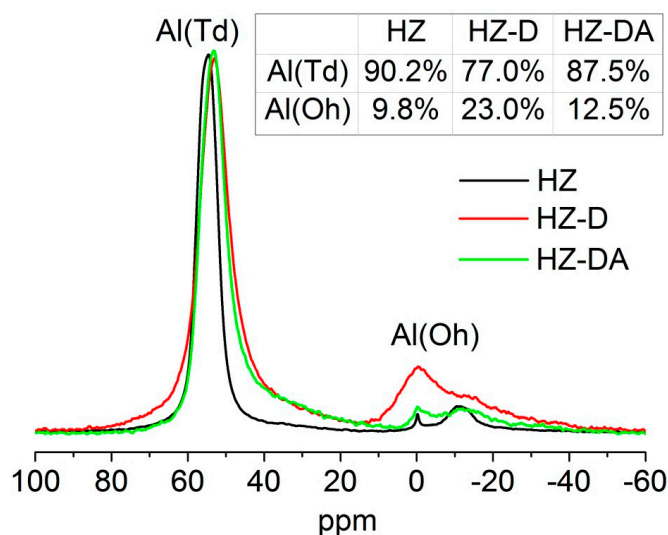
Figure 3. XRD patterns of tested catalysts.

Figure 4. ^{27}Al MAS NMR spectra of tested catalysts.

Figure 5 displays the ^{29}Si resonance, and can be deconvoluted into Si(0Al) at -112 ppm, Si(1Al) at -105 ppm, and Si(3OH) at -99 ppm, respectively. The relative composition of Si(0Al) decreased in the following order: HZ (88.5%) > HZD (87.1%) > HZDA (83.5%), while Si(1Al) and Si(3OH) increased in the order HZ (10.0%) < HZ-D (10.4%) < HZ-DA (10.6%) and HZ (1.5%) < HZ-D (2.5%) < HZ-DA (5.9%), respectively. This fluctuation indicates that Si is etched from the ZSM-5 framework when ZSM-5 is subject to the basic and the acid treatments. Table 2 presents the framework Si/Al ratios ((Si/Al)^F) estimated through the equation proposed by Thomas [27] and the bulk Si/Al composition ((Si/Al)^B) acquired by ICP analysis. The (Si/Al)^F ratio declined monotonically in the following order: HZ (40) > HZ-D (39) > HZ-DA (38), which was in agreement with the above-mentioned trend of decreasing framework Si concentration. The close (Si/Al)^F ratios of tested catalysts implies that the employed alkaline and acid treatments remove mainly amorphous Si and Al species, and the ZSM-5 framework could be preserved. The (Si/Al)^B ratio decreased from 39 (HZ) to 24 (HZ-D) after an alkaline treatment, and then rose to 37 (HZ-DA) after a subsequent acid wash. This fluctuation is related to the dealumination through the acid treatment.
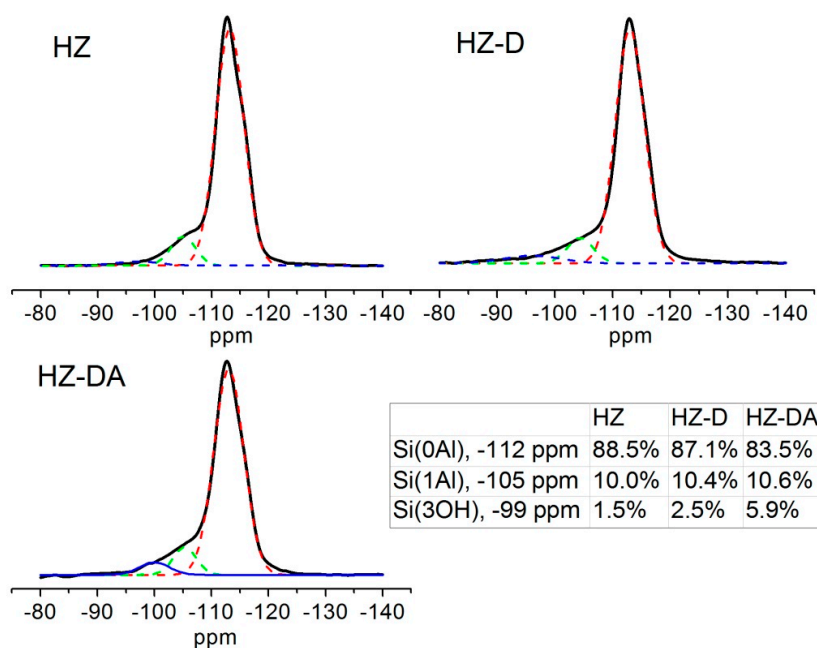
	HZ	HZ-D	HZ-DA
Si(0Al), -112 ppm	88.5%	87.1%	83.5%
Si(1Al), -105 ppm	10.0%	10.4%	10.6%
Si(3OH), -99 ppm	1.5%	2.5%	5.9%

Figure 5. ^{29}Si NMR spectra of tested catalysts. The broken lines are the deconvolution based on a Gaussian function. The relative compositions of Si(0Al), Si(1Al), and Si(3OH) are presented.

Table 2. Compositions and acid concentrations of Lewis and Brønsted acid sites.

Catalyst	(Si/Al)$^{F\ 1}$	(Si/Al)$^{B\ 2}$	Lewis (mmol/g)	Brønsted (mmol/g)
HZ	41	39	0.08	0.26
HZ-D	39	24	0.10	0.14
HZ-DA	38	37	0.05	0.15

[1] Framework Si/Al ratio calculated in ref [27]. [2] Bulk Si/Al ratio estimated by an ICP-AES.

Figure 6 shows the NH$_3$-TPD profiles, and Table 2 lists the acid site densities. Two responses, corresponding to the weak (Lewis) and the strong (Brønsted) acids, could be specified in 170–270 °C and 270–500 °C [28,29]. Compared to the temperature of the maximum desorption rate (T_{max}) of the Lewis acid of HZ (228 °C), HZ-D and HZ-DA had higher T_{max}'s (252 and 250 °C, respectively), this increase in the temperature of desorption was possibly caused by newly-created Lewis acidic Al debris, such as Al(OH$_2$)$^+$ or Al(OH)$^{2+}$ [30,31]. The concentration of the Lewis acid increased from 0.08 mmol/g (HZ) to 0.10 mmol/g (HZ-D), underlining newly-formed Lewis acidic Al on HZ-D. After acid treatment, the Lewis acid concentration decreased to 0.05 mmol/g (HZ-DA), indicating that non-framework Al species can be mostly removed by the acid treatment.

The T_{max} of the Brønsted acid of HZ-D (371 °C) was lower than that of HZ (400 °C), suggesting framework Al can be extracted (dealumination) in the basic condition. A significant decrease of the Brønsted acid concentration from HZ (0.26 mmol/g) to HZ-D (0.14 mmol/g) was also noted. In contrast, the T_{max} of the Brønsted acid of HZ-DA (412 °C) was higher than those of HZ and HZ-D, and a slight increase of the Brønsted site concentration from 0.14 to 0.15 mmol/g was found. This small increase ascertains that small amounts of extracted Al species from the ZSM-5 matrix can be reincorporated into the framework [26].
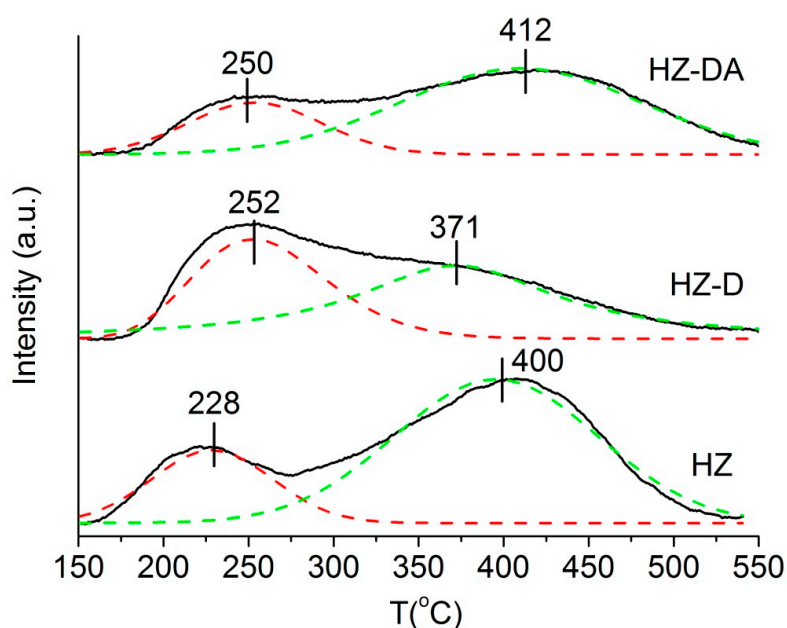
Figure 6. NH_3-TPD profiles of tested catalysts.

Figure 7 shows the TPD of methanol profiles. The desorption of hydrogen, methane, ethylene, methanol, C_3^+ hydrocarbons, and DME were monitored by m/e = 2, 16, 27, 31, 43, and 45, respectively. Desorbed methanol was detected mostly below 200 °C, indicating an operating condition in which methanol conversion had not completed and side reaction should be suppressed [32]. DME was observed in the range from 150 °C to 300 °C, a so-called pre-inition phase of methanol conversion [33], which can be used to interpret the bonding strength of the Brønsted acid [32]. The desorption peak of DME increased with the following trend: HZ-D (230 °C) < HZ (249 °C) < HZ-DA (256 °C), in line with the Brønsted acidity observed from NH_3-TPD. C_3^+ hydrocarbons and ethylene profiles were quite similar; their desorption temperatures were quite close to each other in the temperature range (250–400 °C) of an autocatalysis system [34–36]. Ethylene is a tracer of the arene cycle, while C_3^+ hydrocarbons are produced through the alkene cycle [36–38]. The closely-neighboring desorption temperatures of C_3^+ hydrocarbons and ethylene emphasize that arene and alkene cycled proceed concurrently and are highly interwined [39]. The desorbed CH_4 and H_2 profiles seemed to be coherent, showing two responses in 100–300 °C and 400–700 °C ranges. The low-temperature responses should be related to the contributions of ionized fragments (m/e = 16 and 2) of methanol [40] because the formation of methane and the desorption of dihydrogen are thermodynamically unfavorable below 300 °C [41,42]. Methane originates from the reduction of chemisorbed methoxy species through the hydride transfer [36,42], while dihydrogen should be produced from the combination of two chemisorbed hydrides [41]. Accordingly, the desorption behavior of methane and dihydrogen is associated with hydride mobility. The onset and the peak position of desorbed methane increased in the following order: HZ-D (450 and 545 °C) < HZ (487 and 550 °C) < HZ-DA (510 and 603 °C), which was in line with the trend of desorbed dihydrogen as follows: HZ-D (392 and 545 °C) < HZ (463 and 567 °C) < HZ-DA (481 and 600 °C). This trend underlines that chemisorbed hydride in HZ-D had the highest mobility, while HZ-DA had the lowest one. Since dihydrogen has negligible transfer limitation in micropore channels, and dehydroxylation of the Brønsted acid via the pathway of dehydrogenation is negligible when the temperature is below 600 °C [43], it is rational to hypothesize that there is a correlation between hydride mobility and Lewis acid concentration in the catalyst. That is, the higher the Lewis acid concentration, the more mobile hydride can exist. Thus, aromatic molecules are subsequently formed via the hydride transfer of olefin precursors [36]; therefore, the trend of hydride

mobility may be considered as the indication of the aromatization activity of MTA catalysis on the premise that the space confinement for the cracking of aromatics can be ignored.
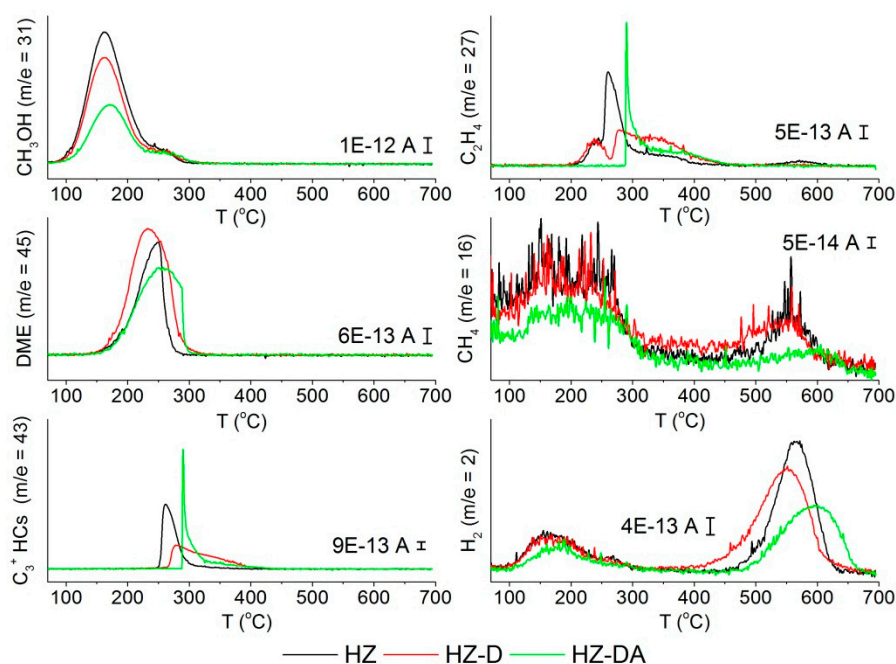

Figure 7. MS spectra of methanol, dimethyl ether, C_3^+ hydrocarbons, ethylene, methane, and hydrogen of TPD of methanol. Reaction conditions: The He stream of 50 mL/min and the heating rate of 20 °C/min.

Table 3 presents the initial conversions and yields of ethylene, propylene, C_4–C_7 hydrocarbons, alkylbenzenes (ABs), and other hydrocarbons of tested catalysts at 400 °C with two different methanol contact times. Detailed distribution of products can be found in Table S1 in Supplementary Materials. Trace DME was detected in the exhaust gas in a shorter contact time (0.24 or 0.17 min * kg_{cat}/mol), while methanol and DME were completely consumed in W/F = 0.49 min * kg_{cat}/mol. No fluctuation of conversion was observed, indicating coking by side reactions such as oligomerization of light olefins should be trivial.

Table 3. Initial conversion and distribution of products at 400 °C with different contact times.

Catalyst	HZ		HZ-D		HZ-DA	
W/F (kg_{cat} * min/mol)	0.24	0.49	0.24	0.49	0.17	0.49
Conversion (%)	99	100	99	100	99	100
C yield (%)						
$C_2^=$	5	6	3	3	4	4
$C_3^=$	21	24	13	12	14	14
C_4–C_7	32	38	31	29	36	33
ABs	40	31	52	55	45	48
Others	2	1	1	1	1	1

Under the condition of W/F = 0.24 or 0.17 min * kg_{cat}/mol, where DME was not fully converted and secondary reactions as the dealkylation and the cracking of aromatics should be restrained [44], the ABs increased in the following order: HZ (40%) < HZ-DA (45%) < HZ-D (52%). In addition to differences in ABs, the major difference between these catalysts is propylene selectivity; HZ produced more propylene (21%) than HZ-D (13%) and HZ-DA (14%) did. Propylene is a major precursor of ABs [45,46] and also a cracked product in arene and olefin cycles [36]; HZ-D is more active than

HZ-DA in propylene aromatization to ABs because both catalysts possess great mesoporosities, but the former is enriched with non-framework Al. This difference is in accordance with the aforementioned hypothesis that non-framework Al species facilitate the hydride transfer and can promote aromatics yields. The low ABs of HZ is mainly attributed to strong space confinement effect, yielding the cracked products (ethylene and propylene) with comparatively higher selectivity.

In a long contact time (W/F = 0.49 kg_{cat} * min/mol), ABs increased from 52% to 55% for HZ-D, 45% to 48% for HZ-DA, but decreased from 40% to 31% for HZ. Moreover, ethylene and propylene were nearly unaltered for HZ-D and HZ-DA, while ethylene and propylene increased from 5% to 6% and from 21% to 24% for HZ, respectively. This rising trend proved that the cracking of ABs prevailed in microporous HZ [18], while transport limitations of HZ-D and HZ-DA were negligible even when the contact time of reactants was increased. Again, HZ-D produced more aromatics than HZ-DA did and far more than HZ did.

Another point that should be addressed is the distributions of C_4–C_7 hydrocarbons, which are generated together with ABs via the intermolecular hydrogen transfer of their precursors, i.e., olefins [45,46]. If the effect of side reactions is trivial, the selectivity of ABs should be positively correlated with that of C_4–C_7 hydrocarbons. However, this is not the case: with increasing contact time, ABs increased and C_4–C_7 hydrocarbons decreased for HZ-D and HZ-DA, whereas HZ showed an opposite trend. A possible explanation for the former trend of HZ-D and HZ-DA is that the promotion of secondary dehydrogenation of C_4–C_7 hydrocarbons, forming dihydrogen and olefins, and subsequently transformed the yielded olefins into ABs [19,20]. As for the latter trend of HZ, the cracking of ABs is imperative. Therefore, the yielded ABs through the intermolecular hydrogen transfer can be broken down into light olefins and cannot reflect the positive correlation between ABs and C_4–C_7 hydrocarbons.

Table 4 presents the initial aromatics selectivity. In different space times, the product selectivities of aromatics were quite similar to one another: C_9 aromatics accounted for more than 50%; durene, 10–25%; the sum of xylenes, 16–25%; toluene, 2–4%; benzene, 0–3%. This indicates that the alkylation/chain growth of aromatic products in MTA depends heavily on the thermodynamics limitation [47]. The main difference is the selectivities of durene and xylenes; HZ-D produced approximately 10% more durene and 8% less xylenes compared to HZ and HZ-DA. Durene has a critical diameter of 0.61 nm; *p*-xylene, 0.58 nm; *o*-xylene and *m*-xylene, 0.68 nm [48]. A shorten diffusion pathway caused by the existence of mesopores can improve durene, *o*-xylene, and *m*-xylene, and suppress *p*-xylene due to the unlashed hurdle of space confinement [18]. However, this is not the case herein because the mesopores of HZ-DA were larger than those of HZ-D (see Figure 1), but HZ-DA generated less durene. Moreover, the micropore PSD (see Figure S2 in Supplementary Materials) showed that the micropore diameter of HZ-DA is approximately 0.61 nm, which is wider than that (0.58 nm) of HZ-D. Hence, the reason why HZ-D produced more durene but less xylenes than HZ-DA did was not that HZ-D was influenced by the reduction of space confinement including the change in the size of mesopores or micropores. The production difference was caused by the different selectivities of durene and xylenes generated by the amorphous Lewis acidic Al on the external surface, which boosted the transalkylation/methylation of aromatics [49], particularly xylenes to form durene. This is also supported by the considerable durene (11–13%) produced by HZ, which has the smallest micropore size (0.55 nm) and a relatively low mesoporosity. Again, the intrinsic Lewis acidic Al sites on the exterior surface of HZ should play a role in durene formation.

In sum, amorphous Lewis acidic Al species of alkali-treated HZSM-5 were essential in enhancing aromatics yields in MTA. The increase of aromatics depends not only on the improved diffusivity caused by the mesopores generated through alkaline treatments, but also on the non-framework Al deposited on the external surface. The improved hydride transfer and methylation/transalkylation activities were discovered on alkali-treated HZSM-5, whereas such an enhancement was absent in its amorphous Al-extracted counterpart.

Table 4. Initial aromatic selectivity at 400 °C with different contact times.

Catalyst	HZ		HZ-D		HZ-DA	
W/F (kg$_{cat}$ * min/mol)	0.24	0.49	0.24	0.49	0.17	0.49
Conversion (%)	99	100	99	100	99	100
Aromatic sel. (%)						
Benzene	2	3	0	2	2	2
Toluene	2	3	2	2	4	4
p- + *m*-xylenes	17	19	12	13	17	18
o-xylene	7	6	4	5	7	6
C$_9$ aromatics	61	56	60	54	59	53
Durene	11	13	22	24	11	17

3. Materials and Methods

3.1. Chemicals

ZSM-5 in NH_4^+ form (CBV 8014, Si/Al = 40) was purchased from Zeolyst International (Conshohocken, PA, USA). Prior to any treatment, the ZSM-5 sample was calcined in static air at 550 °C for 6 h. Standard alkaline treatment (0.2 M NaOH, 65 °C, 30 min, and zeolite-to-liquid ratio = 33 g/L) suitable for MFI zeolites with a Si/Al range of 25 to 50 was employed to prepare mesoporous ZSM-5 [22]. In order to extract non-framework Al, alkali-treated ZSM-5 was subjected to an acid treatment with 0.1 M aqueous HCl at 65 °C for 6 h [22]. All catalysts were subsequently transformed into H^+ form via the ion exchange method [28] before any test. HZSM-5, alkali-treated HZSM-5, and alkali-treated HZSM-5 with subsequent acid treatment were denoted as HZ, HZ-D, and HZ-DA, respectively.

3.2. Catalyst Characterization

The N_2 adsorption isotherm was measured using a ASAP 2020 Plus (Micromeritics Instruments, Norcross, GA, USA) at −196 °C. The sample was degassed at 300 °C for more than 24 h until a pressure of 10^{-3} Pa was reached before the test. The Brunauer-Emmett-Teller (BET) method was used in the relative pressure range of 0.01 to 0.1 to estimate the total surface area (S$_{BET}$), and the *t-plot* method was applied to evaluate microporosity. Pore size distribution (PSD) of micropores was estimated by the desorption branch of the nitrogen isotherm using non-local density functional theory (NLDFT). Scanning electron microscopy (SEM) observations were performed using a Hitachi SU8010 microscope (Tokyo, Japan). X-ray diffraction (XRD) profiles were acquired using a Rigaku D/Max-IIB diffractometer (Tokyo, Japan) operated at 40 kV and 40 mA with Cu Kα radiation. Inductively coupled plasma-atomic emission spectrometry (ICP-AES, Kontron S-35, Augsburg, Germany) was employed to quantify the elemental compositions of Al and Si. The ^{27}Al and ^{29}Si magic-angle-spinning nuclear magnetic resonance (MAS NMR, Bruker Avance 400, Billerica, MA, USA) spectra were obtained at spinning speeds of 10 kHz and 8 kHz in the magnetic field of 9.4 T. The ^{27}Al spectra were recorded using a 3-μs pulse time with a 4 s delay. As for the ^{29}Si spectra, a 3-μs pulse time and a 60 s delay were used. Chemical shifts of ^{27}Al and ^{29}Si were calibrated using 1 M of $[Al(H_2O)_6]^{3+}$ (prepared from aluminum sulfate) and tetramethylsilane as reference. Temperature-programmed desorption (TPD) of ammonia was performed on a chemisorption analyzer (Micromeritics Instruments, AutoChem II) equipped with a thermal conductivity detector (TCD). TPD of methanol was also conducted on the AutoChem II, but was recorded using a quadrupole mass gas analysis system (ThermoStar GSD 320 T, Pfeiffer Vacuum, Aßlar, Germany). Detailed pretreatment and operating conditions of temperature-programmed analyses can be found in recent studies [19,20].

3.3. Reactivity Evaluation

MTA was performed in a continuous fixed-bed system under ambient pressure at 400 °C. Methanol was introduced into an upstream vaporizer at 150 °C via a PU2080 HPLC pump (Jasco Corporation, Tokyo, Japan) with a feeding rate of 0.01 mL/min after achieving a stable feeding rate (mostly after more than 3 h of bypassing). N_2 was set to a flow rate of 60 mL/min as the carrier gas; it could also be used as the internal standard. Approximately 0.07, 0.1, or 0.2 g of a catalyst was consumed per trial, corresponding to the periods of methanol contact time (W/F) of 0.17, 0.24, or 0.49 min * kg_{cat}/mol (the particle sizes range from 177 to 400 μm). Each sample was treated in an air stream (50 mL/min) for 1 h at 500 °C before the test. The exhaust-gas was analyzed by an on-line parallel-dual-column gas chromatograph (GC, SRI Instruments 8610C, Torrance, CA, USA) with a 60 m MXT-1 capillary column and a HeyeSep D packed column. All tubing was kept at 200 °C to avoid condensation. Methanol and dimethyl ether (DME), the dehydrated product of two methanol molecules, were considered as reactants. The reported activity was the averaged results of three data points within the first two hours. Each datum has a carbon mass balance closure higher than 95%. The conversion, yield, and aromatic selectivity were calculated as below:

$$\text{conversion (\%)} = \left(\frac{CH_3OH_{feed} - 2 \times DME_{exhaust}}{CH_3OH_{feed}} \right) \times 100\%$$

$$\text{yield (\%)} = \left(\frac{\text{moles of C atoms in product i}}{\text{sum of C atoms in all products}} \right) \times \left(\frac{CH_3OH_{feed} - 2 \times DME_{exhaust}}{CH_3OH_{feed}} \right) \times 100\%$$

$$\text{aromatic selectivity (\%)} = \left(\frac{\text{moles of C atoms of aromatic product i}}{\text{sum of C atoms in all aromatic products}} \right) \times 100\%$$

4. Conclusions

HZ, HZ-D, and HZ-DA were prepared, characterized, and tested in MTA. HZ-D possesses significant amounts of non-framework Lewis acidic Al species and improved reactant/product diffusivities, both of which are important in elevating aromatics selectivity. The non-framework Al species is discovered to be the key to the enhancement of hydride mobility, which is closely related to aromatics yields in MTA. In addition, concerning distribution of aromatics, the increase in durene and the consumption of xylenes were discovered from the reaction results of HZ-D, but not from those of HZ-DA. This difference emphasized that non-framework Al can boost xylene's methylation/transalkylation to further produce durene with little influence of diffusion limitation.

Author Contributions: Y.-C.L. conceived and designed the experiments, and wrote the paper; P.-C.L., C.-Y.H., and C.-H.C. performed the experiments and analyzed the data.

Conflicts of Interest: The authors declare no conflict of interest.

References

1. Davis, M.E. Ordered porous materials for emerging applications. *Nature* **2002**, *417*, 813–821. [CrossRef] [PubMed]
2. Musilová, Z.; Žilková, N.; Park, S.E.; Čejka, J. Aromatic transformations over mesoporous zsm-5: Advantages and disadvantages. *Top. Catal.* **2010**, *53*, 1457–1469. [CrossRef]
3. Van Donk, S.; Janssen, A.H.; Bitter, J.H.; de Jong, K.P. Generation, characterization, and impact of mesopores in zeolite catalysts. *Catal. Rev.* **2003**, *45*, 297–319. [CrossRef]
4. Tao, Y.; Kanoh, H.; Abrams, L.; Kaneko, K. Mesopore-modified zeolites: Preparation, characterization, and applications. *Chem. Rev.* **2006**, *106*, 896–910. [CrossRef] [PubMed]

5.   Egeblad, K.; Christensen, C.H.; Kustova, M.; Christensen, C.H. Templating mesoporous zeolites. *Chem. Mater.* **2008**, *20*, 946–960. [CrossRef]

6.   Perez-Ramirez, J.; Christensen, C.H.; Egeblad, K.; Christensen, C.H.; Groen, J.C. Hierarchical zeolites: Enhanced utilisation of microporous crystals in catalysis by advances in materials design. *Chem. Soc. Rev.* **2008**, *37*, 2530–2542. [CrossRef] [PubMed]

7.   Holm, M.S.; Taarning, E.; Egeblad, K.; Christensen, C.H. Catalysis with hierarchical zeolites. *Catal. Today* **2011**, *168*, 3–16. [CrossRef]

8.   Verboekend, D.; Perez-Ramirez, J. Design of hierarchical zeolite catalysts by desilication. *Catal. Sci. Technol.* **2011**, *1*, 879–890. [CrossRef]

9.   Mitchell, S.; Pinar, A.B.; Kenvin, J.; Crivelli, P.; Kärger, J.; Pérez-Ramírez, J. Structural analysis of hierarchically organized zeolites. *Nat. Commun.* **2015**, *6*, 8633. [CrossRef] [PubMed]

10.   Chal, R.; Gérardin, C.; Bulut, M.; van Donk, S. Overview and industrial assessment of synthesis strategies towards zeolites with mesopores. *ChemCatChem* **2011**, *3*, 67–81. [CrossRef]

11.   Wei, Y.; Parmentier, T.E.; de Jong, K.P.; Zecevic, J. Tailoring and visualizing the pore architecture of hierarchical zeolites. *Chem. Soc. Rev.* **2015**, *44*, 7234–7261. [CrossRef] [PubMed]

12.   Pérez-Ramírez, J.; Mitchell, S.; Verboekend, D.; Milina, M.; Michels, N.-L.; Krumeich, F.; Marti, N.; Erdmann, M. Expanding the horizons of hierarchical zeolites: Beyond laboratory curiosity towards industrial realization. *ChemCatChem* **2011**, *3*, 1731–1734. [CrossRef]

13.   Liang, T.; Chen, J.; Qin, Z.; Li, J.; Wang, P.; Wang, S.; Wang, G.; Dong, M.; Fan, W.; Wang, J. Conversion of methanol to olefins over h-zsm-5 zeolite: Reaction pathway is related to the framework aluminum siting. *ACS Catal.* **2016**, *6*, 7311–7325. [CrossRef]

14.   Lietz, G.; Schnabel, K.H.; Peuker, C.; Gross, T.; Storek, W.; Völter, J. Modifications of H-ZSM-5 catalysts by naoh treatment. *J. Catal.* **1994**, *148*, 562–568. [CrossRef]

15.   Holm, M.S.; Svelle, S.; Joensen, F.; Beato, P.; Christensen, C.H.; Bordiga, S.; Bjørgen, M. Assessing the acid properties of desilicated zsm-5 by ftir using co and 2,4,6-trimethylpyridine (collidine) as molecular probes. *Appl. Catal. A* **2009**, *356*, 23–30. [CrossRef]

16.   Song, Y.; Zhu, X.; Song, Y.; Wang, Q.; Xu, L. An effective method to enhance the stability on-stream of butene aromatization: Post-treatment of zsm-5 by alkali solution of sodium hydroxide. *Appl. Catal. A* **2006**, *302*, 69–77. [CrossRef]

17.   Mochizuki, H.; Yokoi, T.; Imai, H.; Namba, S.; Kondo, J.N.; Tatsumi, T. Effect of desilication of h-zsm-5 by alkali treatment on catalytic performance in hexane cracking. *Appl. Catal. A* **2012**, *449*, 188–197. [CrossRef]

18.   Bjørgen, M.; Joensen, F.; Spangsberg Holm, M.; Olsbye, U.; Lillerud, K.-P.; Svelle, S. Methanol to gasoline over zeolite h-zsm-5: Improved catalyst performance by treatment with naoh. *Appl. Catal. A* **2008**, *345*, 43–50. [CrossRef]

19.   Lai, P.-C.; Chen, C.-H.; Lee, C.-H.; Lin, Y.-C. Methanol conversion to aromatics over ga–supported hzsm-5 with evolved meso- and microporosities by desilication. *ChemistrySelect* **2016**, *1*, 6335–6344. [CrossRef]

20.   Lai, P.-C.; Chen, C.-H.; Hsu, H.-Y.; Lee, C.-H.; Lin, Y.-C. Methanol aromatization over ga-doped desilicated hzsm-5. *RSC Adv.* **2016**, *6*, 67361–67371. [CrossRef]

21.   Groen, J.C.; Pérez-Ramírez, J. Critical appraisal of mesopore characterization by adsorption analysis. *Appl. Catal. A* **2004**, *268*, 121–125. [CrossRef]

22.   Verboekend, D.; Mitchell, S.; Milina, M.; Groen, J.C.; Pérez-Ramírez, J. Full compositional flexibility in the preparation of mesoporous mfi zeolites by desilication. *J. Phys. Chem. C* **2011**, *115*, 14193–14203. [CrossRef]

23.   Kulkarni, S.B.; Shiralkar, V.P.; Kotasthanc, A.N.; Borade, R.B.; Ratnasamy, P. Studies in the synthesis of zsm-5 zeolites. *Zeolites* **1982**, *2*, 313–318. [CrossRef]

24.   Brunner, E.; Ernst, H.; Freude, D.; Fröhlich, T.; Hunger, M.; Pfeifer, H. Magic-angle-spinning nmr studies of acid sites in zeolite H-ZSM-5. *J. Catal.* **1991**, *127*, 34–41. [CrossRef]

25.   Groen, J.C.; Peffer, L.A.A.; Moulijn, J.A.; Pérez-Ramírez, J. Mechanism of hierarchical porosity development in mfi zeolites by desilication: The role of aluminium as a pore-directing agent. *Chem. Eur. J.* **2005**, *11*, 4983–4994. [CrossRef] [PubMed]

26.   Verboekend, D.; Pérez-Ramírez, J. Desilication mechanism revisited: Highly mesoporous all-silica zeolites enabled through pore-directing agents. *Chem. Eur. J.* **2011**, *17*, 1137–1147. [CrossRef] [PubMed]

27.   Thomas, J.M. Dealuminated zeolites. *J. Mol. Catal.* **1984**, *27*, 59–69. [CrossRef]

28. Fanchiang, W.-L.; Lin, Y.-C. Catalytic fast pyrolysis of furfural over H-ZSM-5 and ZN/H-ZSM-5 catalysts. *Appl. Catal. A* **2012**, *419*, 102–110. [CrossRef]

29. Lónyi, F.; Valyon, J. On the interpretation of the NH$_3$-TPD patterns of H-ZSM-5 and H-mordenite. *Microporous Mesoporous Mater.* **2001**, *47*, 293–301. [CrossRef]

30. Meshram, N.R.; Hegde, S.G.; Kulkarni, S.B. Active sites on ZSM-5 zeolites for toluene disproportionation. *Zeolites* **1986**, *6*, 434–438. [CrossRef]

31. Woolery, G.L.; Kuehl, G.H.; Timken, H.C.; Chester, A.W.; Vartuli, J.C. On the nature of framework brønsted and Lewis acid sites in ZSM-5. *Zeolites* **1997**, *19*, 288–296. [CrossRef]

32. Hunger, B.; Matysik, S.; Heuchel, M.; Einicke, W.-D. Adsorption of methanol on ZSM-5 zeolites. *Langmuir* **1997**, *13*, 6249–6254. [CrossRef]

33. Schulz, H.B.; Böhringer, W.; Zhao, S. Comparison of shape selectivity of coke formation in different zeolites. In Proceedings of the 9th International Zeolite Conference, Montreal, QC, Canada, 5–10 July 1992; von Ballmoos, R., Higgins, J.B., Treacy, M.M.J., Eds.; Butterworth-Heinemann: Montreal, QC, Canada, 1993; p. 567.

34. Ono, Y.; Mori, T. Mechanism of methanol conversion into hydrocarbons over ZSM-5 zeolite. *J. Chem. Soc. Faraday Trans. 1* **1981**, *77*, 2209–2221. [CrossRef]

35. Schulz, H.; Siwei, Z.; Kusterer, H. Autocatalysis, retardation, reanimation and deactivation during methanol conversion on zeolite HZSM-5. *Stud. Surf. Sci. Catal.* **1991**, *60*, 281–290.

36. Sun, X.; Mueller, S.; Liu, Y.; Shi, H.; Haller, G.L.; Sanchez-Sanchez, M.; van Veen, A.C.; Lercher, J.A. On reaction pathways in the conversion of methanol to hydrocarbons on HZSM-5. *J. Catal.* **2014**, *317*, 185–197. [CrossRef]

37. Olsbye, U.; Svelle, S.; Bjørgen, M.; Beato, P.; Janssens, T.V.W.; Joensen, F.; Bordiga, S.; Lillerud, K.P. Conversion of methanol to hydrocarbons: How zeolite cavity and pore size controls product selectivity. *Angew. Chem. Int. Ed.* **2012**, *51*, 5810–5831. [CrossRef] [PubMed]

38. Teketel, S.; Westgard Erichsen, M.; Lonstad Bleken, F.; Svelle, S.; Petter Lillerud, K.; Olsbye, U. *Shape Selectivity in Zeolite Catalysis. The Methanol to Hydrocarbons (mth) Reaction*; The Royal Society of Chemistry: London, UK, 2014; Volume 26, pp. 179–217.

39. Ilias, S.; Khare, R.; Malek, A.; Bhan, A. A descriptor for the relative propagation of the aromatic- and olefin-based cycles in methanol-to-hydrocarbons conversion on H-ZSM-5. *J. Catal.* **2013**, *303*, 135–140. [CrossRef]

40. NIST Chemistry Webbook. Available online: http://webbook.nist.gov/cgi/cbook.cgi?ID=C67561&Units=SI&Mask=200 (accessed on 20 July 2017).

41. Derouane, E.G.; Abdul Hamid, S.B.; Ivanova, I.I.; Blom, N.; Højlund-Nielsen, P.-E. Thermodynamic and mechanistic studies of initial stages in propane aromatisation over ga-modified H-ZSM-5 catalysts. *J. Mol. Catal.* **1994**, *86*, 371–400. [CrossRef]

42. Schulz, H. "Coking" of zeolites during methanol conversion: Basic reactions of the mto-, mtp- and mtg processes. *Catal. Today* **2010**, *154*, 183–194. [CrossRef]

43. Yun, J.H. Structure and Reactivity of Dehydroxylated Bronsted Acid Sites in H-ZSM-5 Zeolite: Generation of Stable Organic Radical Cation and Catalytic Activity for Isobutane Conversion. Mater's Thesis, University of Delaware, Newark, NJ, USA, 2011.

44. Khare, R.; Bhan, A. Mechanistic studies of methanol-to-hydrocarbons conversion on diffusion-free mfi samples. *J. Catal.* **2015**, *329*, 218–228. [CrossRef]

45. Stöcker, M. Methanol-to-hydrocarbons: Catalytic materials and their behavior. *Microporous Mesoporous Mater.* **1999**, *29*, 3–48. [CrossRef]

46. Conte, M.; Lopez-Sanchez, J.A.; He, Q.; Morgan, D.J.; Ryabenkova, Y.; Bartley, J.K.; Carley, A.F.; Taylor, S.H.; Kiely, C.J.; Khalid, K.; et al. Modified zeolite ZSM-5 for the methanol to aromatics reaction. *Catal. Sci. Technol.* **2012**, *2*, 105–112. [CrossRef]

47. Cai, D.; Wang, Q.; Jia, Z.; Ma, Y.; Cui, Y.; Muhammad, U.; Wang, Y.; Qian, W.; Wei, F. Equilibrium analysis of methylbenzene intermediates for a methanol-to-olefins process. *Catal. Sci. Technol.* **2016**, *6*, 1297–1301. [CrossRef]

48. Chang, C.D. Hydrocarbons from methanol. *Catal. Rev.* **1983**, *25*, 1–118. [CrossRef]

49. Zhang, J.; Qian, W.; Kong, C.; Wei, F. Increasing para-xylene selectivity in making aromatics from methanol with a surface-modified ZN/P/ZSM-5 catalyst. *ACS Catal.* **2015**, *5*, 2982–2988. [CrossRef]